A STATISTICAL ANALYSIS OF THE DYNAMIC RESPONSE OF A RAILWAY VIADUCT

André H. Jesus[a], Zuzana Dimitrovová[a,*], Manuel A.G. Silva[a]

[a]*Department of Civil Engineering, Faculdade de Ciências e Tecnologia, Universidade Nova de Lisboa, 2829-516 Caparica, Portugal*

Abstract

A statistical analysis of the dynamic response of a railway viaduct, modelled after an actual structure, is presented. The finite element model of the viaduct is based on the data provided by the Portuguese Railway Company REFER EPE. The train load is simplified by a set of constant moving forces and the range of velocities implemented corresponds to typical velocities of circulation. The viaduct is composed of eight modules, but, for the sake of simplicity, only the first viaduct module is included in the analysis.

In order to perform the statistical analysis, the viaduct is subjected to a two-level factorial design. It is shown that key parameters cannot be analysed individually because in some cases interaction effects can be more important than single effects.

Response functions of significant results are presented. Their usage for dynamic response estimates is exemplified. Further it is shown how they can be used for the determination of a probability that a certain value of interest is exceeded, provided the range of key parameters corresponds to the interval of uncertainties, where the true value obeys the normal distribution.

This type of straightforward application of statistical analysis highlights the interaction of adequately selected key parameters, provides useful information for design guidelines and is believed to lead to better planning and more realistic representation of the actual response of railway bridges.

Keywords: dynamic analysis, railway bridges, resonance, factorial design, residuals, response function

1. Introduction

1.1. General

Railway bridges are important connecting infrastructures that require specific design considerations supported by an adequate numerical modelling. The wide range of factors that influence the design, followed by the choice of the adequate numerical procedure, requires a fair amount of simplifications of this complex system.

Deterministic analyses of complex engineering structures can lead to wrong conclusions, because of uncertainties in the input data. Therefore a statistical treatment of input as well as output should be accomplished. In this context determination of key input data governing the dynamic response of the system is extremely important. Numerical models usually require calibration measurements to achieve the model/structure agreement. However, field measurements are also subject to experimental error.

Although simplified models of railway tracks are widely used, the growth in numeric and computational efficiency made complete models

*Corresponding author

Email addresses: andrehjesus@gmail.com (André H. Jesus), zdim@fct.unl.pt (Zuzana Dimitrovová), mgs@fct.unl.pt (Manuel A.G. Silva)

involving several structural details feasible and preferable. The computational speed is a very important factor and based on hardware and algorithmic efficiency has been constantly improving over the years. Therefore, some computationally intensive statistical methods have become usable. Statistical methods can enhance the analysis by providing results that are more realistic, and consequently give a better insight on the situation of interest and help in the calibration of the models.

1.2. Bridge and train models

Over the last centuries various types of bridge models have been developed to address the fundamental problems of bridge dynamics. Due to the rich history and considerable extent of the topic a general review would be unnecessarily lengthy. The progress in numerical methods, like the finite element (FE) method, presents very accurate and efficient modeling of complex mechanisms [1]. The components of the bridge and railway track can be modelled in a simpler or a more sophisticated manner depending on the objectives of the model [2].

There are essentially two cases of dynamic models: either with continuously distributed mass, or with lumped masses along the length of the bridge. Other models implement a combination of those two approaches. Some of the continuum models of simply-supported Euler-Bernoulli beams [2, 3, 4] were by far the most popular, due to their simplicity and ability to lead to closed-form solutions. These models are still frequently used, e.g. in the analysis of a bridge-track-train interaction [5]. Despite the fact that these continuum models are a good first approximation of the bridge system, their practical applicability is limited to bridges of simple configuration.

There are mainly three types of models with regard to loading: (i) the moving force model [6, 7]; (ii) the moving mass model [8, 9]; and (iii) the moving system model [10, 11] that comprehends a system of masses, springs and dampers. In the present work the moving force model can be safely used since the ratio of the moving mass load over the mass of the bridge does not exceed 30 % and the load velocity will not reach 20 % of the critical one, as shown by parametric analysis [12]. This simplification was already used in the authors' previous work [13] and it is also mentioned in the monographs [1, 2].

1.3. Design of experiments

To idealise railway bridges the associated components of the structure are subject to certain simplifications and the input data to a related numerical model are supplied with a certain level of uncertainty. The additional overall complexity of the problem can significantly mislead the calculated response when deterministic models are employed. Statistical method analyses implement data within a certain range and consequently the calculated response is determined with a certain probability of occurrence giving a better insight of this problem. This approach of combined dynamic response of bridges with statistical treatment by design of experiments is under growth in the scientific community. It can be found in [14] and related works of the first author. In Karalar [15] statistical methods are applied to the analysis of isolation of bridges. Structural health monitoring (SHM) on bridges is another field of structural engineering that is currently employing statistical treatment [16, 17].

Previous works addressing parametric analyses of railway bridges considered the influence of key parameters (factors) individually. It is clearly shown in many statistical publications [18, 19, 20] that this one-variable-at-a-time strategy fails frequently because it tacitly assumes that the maximising value of one variable is independent of the level of the other. Simultaneous consideration of the influence of several key parameters provides a better representation of reality.

Statistical analysis of numerical results allows to define a set of key input data and key results, in order to study complex mechanisms interactions and understand if the involved factors play a role in the response in an interactive or simply additive way. Key factors are selected by the user and the factorial experiment stands for the statistical analysis of the variance of the results due to the changes in the key input data. One of the possible usage of such outcomes is the calibration of nu-

merical models. Then the determined key results identify the characteristics to be measured by in-situ experiments [21] and the key input data serve for model calibration. The experimental design, if adequately adjusted to the situation can reduce significantly the experimental error. Another usage, implemented in this paper, is to consider the variations of key input data in accordance with the uncertainty of the actual values, i.e. to assume that the key input value occurrence within the specified interval verifies the normal distribution with the mean coincident with the middle value. Associated standard deviation has to ensure negligible probability outside this interval. Then from the approximate response function it is possible to determine the probability of exceedance of a certain result depicted by the user.

Dynamic analysis of a viaduct involves a large number of variables and is therefore unsuitable for a direct factorial analysis. It is preferable to run several parametric studies first and gradually select the most relevant factors. In a previous work [13] ballast stiffness, concrete stiffness, soil stiffness, train speed, ballast damping and rail-pad damping were selected as key factors. In this context the concrete stiffness is represented by Young's modulus. The main conclusions regarding peak displacements revealed dominance of single effects, led by the concrete stiffness for displacements at the deck level and by the train speed for displacements at the soil level. Peak accelerations showed strong interactions between factors led by the train speed and its interaction with the ballast stiffness. It was concluded that this interaction deserves more attention, which is conducted in this paper. Due to the fact that the influence of the concrete modulus is obvious and affects significant part of the model, this factor was omitted and attention was focused on the railway superstructure. It is shown that the superstructure parameters can influence significantly the global behaviour. In order to detail the ballast stiffness interaction with the train speed, also dynamically activated ballast mass, ballast constitutive model and damping are included in the analysis. The ballast behaviour model is considered in this paper as the only qualitative factor. Only one single force and one value for the reference train speed 180 km/h was used in [13]. Hence, special attention is placed here on the train speed and on a more realistic train model.

The question of whether the train speed is a valid factor in the two-level factorial analysis is addressed in detail. It is known (e.g. Yang [1]) that structures subjected to repetitive moving loads increase their dynamic response at resonance speed. The analysis presented in Yang [1] is valid for simply supported beam representing the bridge. This analysis can be extended to double beam with an elastic layer. Results are not easily obtainable analytically, but a simple model can be tested numerically. Details of this analysis are given in Section 4.1. It was concluded that within the range of typical train velocities it is safe to perform two-level factorial design, where one of the factors is the train speed.

Given the summary above the objectives and new contributions of this paper are:

(i) To check the existence of new dominating factors and interactions that influence the dynamic response results with importance on the superstructure;
(ii) To show numerically that interaction effects can be more important than single effects;
(iii) To establish the final response function and to calculate the probability of exceeding a certain value of interest.

2. The Santana do Cartaxo viaduct

Train specification and in-situ measurements of the soil foundation properties were supplied by REFER EPE [22]. The case study refers to a location in the Portugal North Line, second sublink Setil Sul Vale de Santarém, which develops from km $56 + 625$ until km $65 + 287$ and is part of the rehabilitation of the North Line. The Santana do Cartaxo segment, where a new railway was included over a viaduct built at km $59 + 000$ to km $60 + 000$ (Figure 1) is an exception in the rehabilitation, which otherwise follows closely the original railway route design. A more detailed description of the structure can be found in previous work of the authors [13].

(a) General view

(b) Embankment

Figure 1: Santana do Cartaxo viaduct

The viaduct is composed by a set of eight module sections in the longitudinal direction. Each module is connected to the other through transition pillars which are larger and have more piles than the intermediate pillars. Designating by ascending direction (AD) the one from south to north and by (DD) the descending and opposite one, then the first of the eight modules comprises three spans of 25, 30, and 25 m, finalizing a length of 80 m, while the other seven modules have spans of 25, 4×30 and 25 m, yielding the length of 170 m, bringing the total viaduct length to 1312 m. On the plan view (see Figure 2) the viaduct develops linearly and at the end starts a left transition curve of 1750 m radius.

The geological layers are visualised in Figure 2. Material properties were obtained by in-situ measurements and are given in Appendix A. The alluvium layer is divided in three geologically different

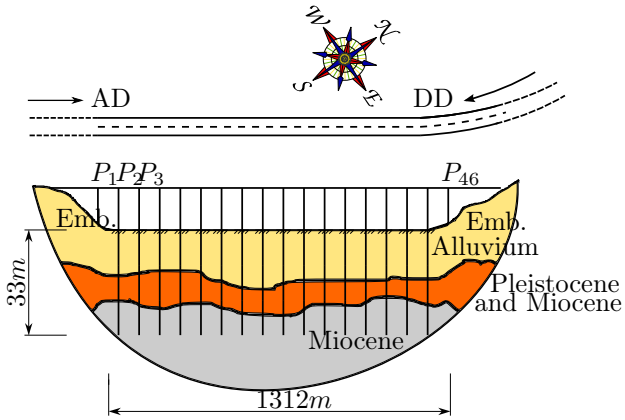

Figure 2: Viaduct top and left view

categories A1, A2 and A3, but regarding their mechanical properties they can be grouped in two categories A1 and A2/A3. For the sake of simplicity, in this paper a single layer with average properties is considered.

The traffic over the viaduct is practically equally distributed between Alfa Pendular and Intercidades trains (Figure 3). Travelling speeds can be seen in Table 1.

	Locomotive	Mass [ton]	Speed [km/h]
Merchandise TAKARGO	LE-4700	87	100
Passengers Intercidades	CP-5600	87	190 (AD); 180 (DD)
Passengers Alfa Pendular	CP-4000	58	190 (AD); 180 (DD)

Table 1: Circulation characteristics

The Intercidades train was selected to perform analyses in this paper.

3. Finite element model

3.1. General considerations

The numerical model is developed with the ANSYS/LS-DYNA module. The parametric analyses with automatic extraction of key results are coded with APDL (ANSYS parametric design language) [23].

For the sake of simplicity, only the first of the eight modules, the one having three spans of 25,

(a) CP-5600 Locomotive

(b) Corail carriage

Figure 3: Train photos

30 and 25 m, is modelled. This module is supported at its ends on one embankment and one transition pillar that connects it with the rest of the viaduct. The other seven modules were modelled by representative spring and dampers. Bending natural frequencies were used as a base for checking the accuracy of the modulation, because bending vibration modes have decisive contribution to the dynamic response. As the model is fully parametric it was easy to compare natural bending frequencies of an arrangement constituted by either one or two modules, and they were found sufficiently proximate.

Several structural simplifications, generally adopted by other researches, that keep the computational effort at a tractable level were introduced. Rail-pads and ballast are represented by linear and rotational spring and damper elements acting in three directions. The arrangement is a three-dimensional extension of the system used in [24] and it is displayed in Figure 4.

Rails, sleepers, pillars, foundation blocks and piles have one dominant dimension and therefore are approximated by beam elements. Low thickness with respect to cross section of the viaduct deck justifies implementation of shell elements on the viaduct deck. The viaduct pillars are modelled with a rectangular section and connected at the top to the shell elements that represent the lower deck. The connection allows for rotation around an horizontal axis parallel to the sleepers. The piles and foundation block are idealised as a pair of beams connected by a third concrete block. Beam elements are superposed directly on the edges of soil elements to avoid additional constraints. Only a part of the soil layers is included and modelled by three-dimensional elements. The surrounding soil is substituted by representative springs and dampers. Springs represent the rigidity of the surrounding layers and dampers ensure smooth wave propagation into surrounding layers without reflections from the artificial boundary. The method of coefficients estimation of these representative springs and dampers and their validation is presented in the previous work [13]. Some remarks are also included in Appendix C. Springs and dampers are also used to model the embankments.

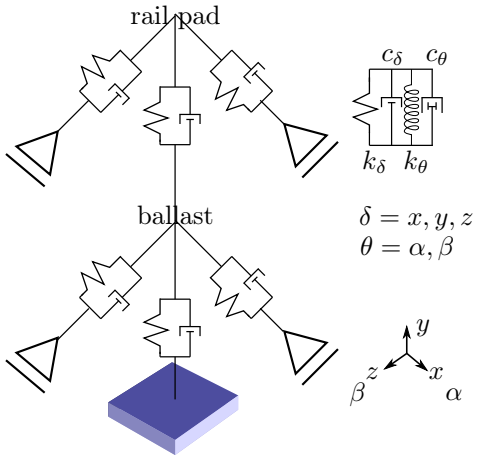

Figure 4: Spring-damper ballast system

All input data used in the numerical analyses

are summarised in Appendix A, B and C.

3.2. Modal analysis

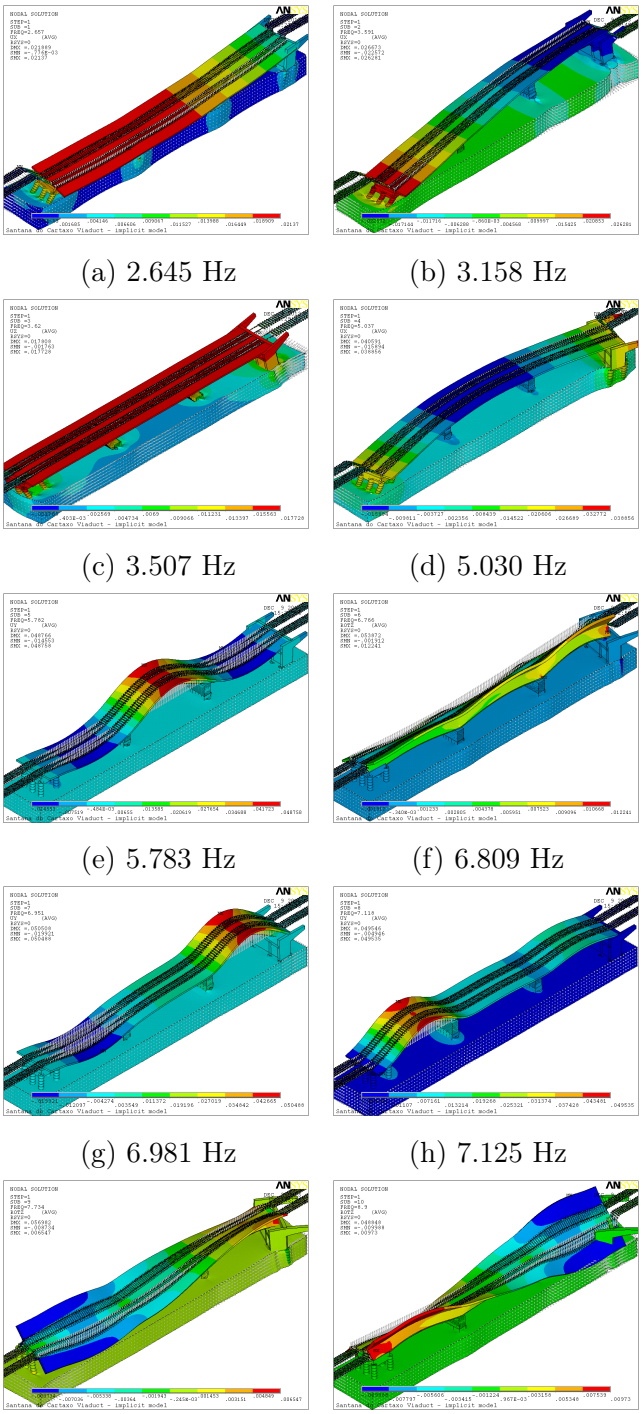

(a) 2.645 Hz (b) 3.158 Hz

(c) 3.507 Hz (d) 5.030 Hz

(e) 5.783 Hz (f) 6.809 Hz

(g) 6.981 Hz (h) 7.125 Hz

(i) 8.160 Hz (j) 9.392 Hz

Figure 5: Mode shapes

The ten first mode shapes are illustrated in Figure 5. The first three bending modes are the 5th, the 7th and the 8th mode, respectively, shown in Figure 5e, g and h. A simple check shows that the value of 5.78 Hz is comparable with the approximate value, obtained for a simply supported beam corresponding to the middle span.

The modal analysis was also used to certify the representative stiffnesses of the lateral springs. For numerical values consult Appendix C.

3.3. Experimental validation

The adequacy of the finite element model is being confirmed experimentally by in-situ measurements. Detailed analyses will be submitted as a separate research paper. The first indication of the validity of the numerical model and results is the confirmation of the first bending frequency. Velocity profiles were measured by geophone sensors during train passages and transformed by Fourier transformation into frequency domain. The extraction point of this result is located at the deck level inside the central span of the module on a small containing wall located at 4.4 m from the viaduct central axis. The sensor was glued to the wall in order to avoid relative slips and inherent vibrations of the device.

It is seen in Figure 6 that the experimentally measured first bending frequency is around 5.72 Hz, the one from the explicit model indicates 5.63 Hz, and the implicit model gives 5.78 Hz. It is noted that the ANSYS explicit module does not perform modal analysis and the estimate was obtained by Fourier transformation of the velocity results. The value of 5.63 Hz includes the effect of damping, differently from the implicit model.

It is also worthwhile to add that geophone measures are not viable below 2 Hz and therefore these values are not shown.

This validation also confirms that viaduct modules do not interfere significantly and thus it is possible to analyse them separately.

3.4. Nonlinear ballast behaviour

Ballast behaviour was selected as a qualitative factor for the factorial design and a nonlinear behaviour (high level) was tested against the linear one (low level). All the ballast springs are assumed to have either linear or nonlinear behaviour. A type of nonlinear behaviour curve

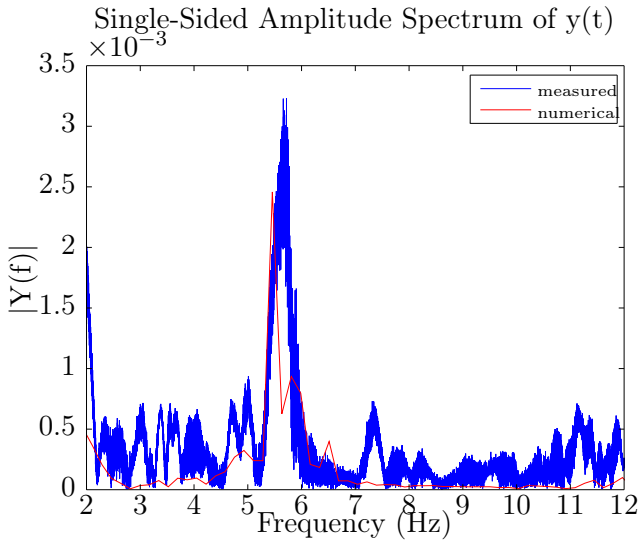

Figure 6: Numerically and experimentally obtained velocity in frequency domain

and a connection between the linear and nonlinear behaviours was established. According to [25], the appropriate function describing the nonlinear ballast behaviour has a cubic polynomial form. The parameters (coefficient with the linear $\tilde{K}_l$ and cubic terms $\tilde{K}_c$), that govern the nonlinear behaviour were calculated from two conditions: (i) same elastic force at a given displacement and (ii) same elastic energy accumulated at a given displacement. The linear elastic force in the former condition was reduced to 90 %, thus:

$$\begin{cases} 0.9\mathrm{F}_l(\delta_1) = \mathrm{F}_c(\delta_1) \\ U_l(\delta_2) = U_c(\delta_2) \end{cases} \tag{1}$$

where F_l and F_c represent the elastic forces, and U_l and U_c stand for the accumulated energy in the linear and nonlinear (cubic) springs, respectively, and δ_1 and δ_2 are the specified displacements. Displacement δ_2 was chosen as a typical displacement of 1 mm and δ_1 as 50 % of δ_2, i.e. 0.5 mm. It was verified numerically that changing δ_2 does not affect the results significantly.

Solving the equations for the coefficients of the cubic spring, one gets:

$$\begin{cases} \tilde{K}_l = \frac{0.1K_l(-20\delta_1^2+9\delta_2^2)}{-2\delta_1^2+\delta_2^2} \\ \tilde{K}_c = \frac{0.2K_l}{-2\delta_1^2+\delta_2^2} \end{cases} \tag{2}$$

The graph in Figure 7 presents a typical force displacement relation of the linear and cubic springs related to the vertical spring, i.e. when K_l is equal to 120000 kN/m.

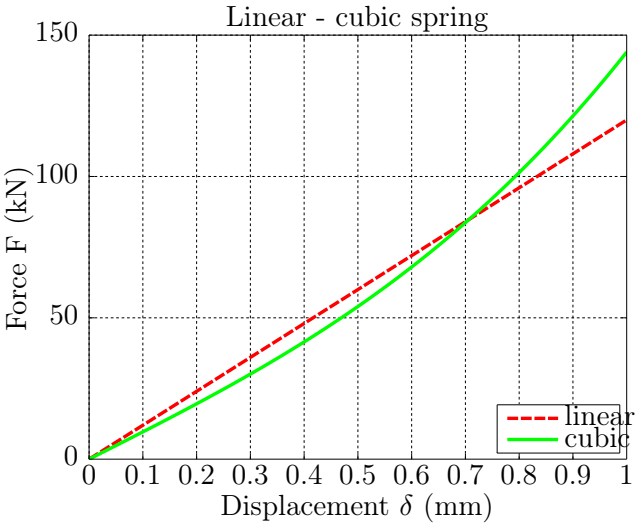

Figure 7: Cubic (solid green) and linear (dashed red) spring force-displacement graph

4. Results

Explicit analysis is performed with LS-DYNA software with a time step calculated according to the element sizes and properties as 0.017 ms. The full train needs 4.47 s to traverse the model at the speed of 185 km/h, which would imply an excessive number of results to be filed. Therefore only results from 500 selected files are saved and results are not available for all times. The model has 64878 elements and each analysis took around 2 h and a half for the speed of 185 km/h and around 2 h for the speed of 195 km/h. Mesh size is variable over the model; it gradually increases from 10 cm in rail to 1 m in soil. Small elements in rails were chosen in a way that allows adequate representation of the rail deformation between sleepers. It was verified numerically that soil elements are sufficiently small.

4.1. Resonance parametric analysis

In this section results of parametric analyses with respect to the velocity of the moving load

are shown in order to confirm that there is no increase of the structural response within the interval of analysed train velocities. Factors variation is given in the next section, but it is advanced that two reference velocities were selected with 2.7 % variation covering approximately the interval from 180 to 200 km/h, which corresponds to the range of true operating velocities.

The critical velocity v_{cr} of a load moving on a simply supported beam is derived e.g. in Frýba [4] as:

$$v_{cr} = 2 f_1 L \tag{3}$$

where f_1 is the fundamental frequency and L is the beam length. By using the numerical value of 5.63 Hz, which corresponds to the first bending mode and essentially excites the middle span of 30 m length, the critical velocity yields 337.8 m/s=1216 km/h. Therefore the critical velocity of a single load is not of concern. Note that in this case it makes more sense to use the first frequency from the explicit model.

Resonance resulting from the successive passage of equidistant loads or groups of loads was analysed by several authors. The analysis given in monograph [1] is valid for simply supported beams. The resonance velocity $v_{n,j}^{res}$ is derived as:

$$v_{n,j}^{res} = \frac{f_n d}{j} \tag{4}$$

where d is the distance between the loads, f_n is n-th natural frequency in Hz and j is an integer (see Figure 8). In such a case the deflection

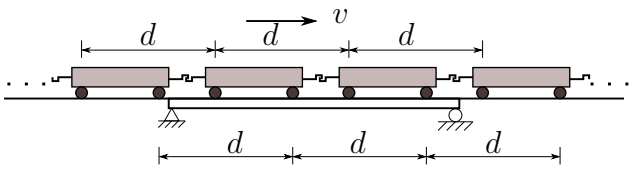

Figure 8: The model of simply supported beam under a moving train, adapted from [1]

shape is first mode dominant, the contributions of other modes decrease with $1/n^2$ and therefore only $n = 1$ can be considered. For the same reason also the second resonant velocity ($j = 2$) is not very important and does not produce significant response increase, especially in downward oriented displacement.

It is known that simply supported beam on elastic foundation behaves differently, the order of the mode having the highest contribution can be calculated as the closest integer verifying

$$j_{cr} = \frac{L}{\pi} \sqrt[4]{\frac{k}{EI}} \tag{5}$$

where k is the stiffness of the foundation and EI is the bending stiffness of the beam. The drop in other modes contributions is not so significant as in the previous case [26]. In a mixed case of double beam with an elastic layer where the lower beam represents the deck, the upper beam the rail and the elastic core stands for the ballast, conclusions are dependent on the relative stiffnesses.

In our case, due to the high bending stiffness of the viaduct deck, ballast springs and the upper beam (rail) have very small influence on the natural frequencies and relative modes contributions. It was verified numerically on a simple finite element model of the corresponding double beam, that the response is again first mode dominant and, for instance, the third mode frequency is only less than 3 % below the third frequency of an equivalent simply supported beam. The deflection shape of the rail resembles the deflection of a beam on an elastic foundation superposed to the global deck deflection, that is dominant. The extreme values are again governed by the first natural frequency as in the case of a simply supported beam described above. For this reason the formula (4) can be used.

The distance between bogies in the Intercidades locomotive CP-5600 and in the carriages is 10.5 m and 18 m, respectively. The length d from Figure 8 is 26.4 m. This means that for $f_1 = 5.63$ Hz, velocities of 59.1 m/s=213 km/h, 101.3 m/s=365 km/h and 148.6 m/s=535 km/h should be tested for possible resonance. It is seen that only the first value is close to the range of operating velocities.

The maximum downward displacement of the middle point of the middle span on the external rail subjected to the load was extracted in para-

metric analysis where the velocity variation step was 1 km/h. The numerically obtained velocity that induces the highest value is 205 km/h (see Figure 9a), which is quite close to the analytically determined velocity of 213 km/h. It is seen that the variation of the maximum displacement within a much larger range of velocities than the one examined is only around 4 % and therefore negligible. Larger variations would be seen in upward displacements, but this was not analysed in this paper. From the factors considered in this paper the ones that influence the natural frequencies and consequently the resonance peaks in velocities are the ballast stiffness and the dynamically activated ballast mass. Considering these variations, the first bending frequency suffers changes only within 0.5 % and thus the same change is transferred to the resonance velocities. This change, however, still places the low resonance peak outside the examined interval.

In Figure 9b the deflection curves for subsequent velocities from 197 km/h to 206 km/h are plotted. It is seen that there is no increase of the response as subsequent loads are passing. Also, the residual response, i.e. the response of the middle point when the load is over the bridge, does not present excessive values. There is a sudden change in displacement shape of the curve related to 200 km/h, but local extreme values are not significantly different and thus it can be considered that the smooth changing in the velocity induces smooth changing in the response, confirming that the two-level factorial analysis with one of the factors being the train velocity can produce valid results. The effect of resonance is not pronounced due to the vertical flexibility of the supports (pillars), which generally smoothes the resonance response, and, in addition, by influence of the other spans that act as rotational springs at the simple supports of the middle span.

4.2. Statistical analysis

The statistics toolbox of Matlab [27] was used to produce deviation plots of single effects and interactions from a reference normal distribution, response functions and residuals diagnostic checks.

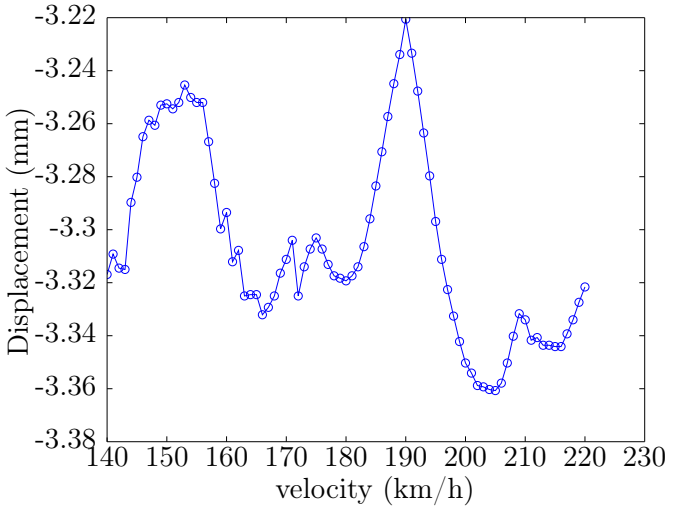

(a) Maximum downward displacement variation in middle point

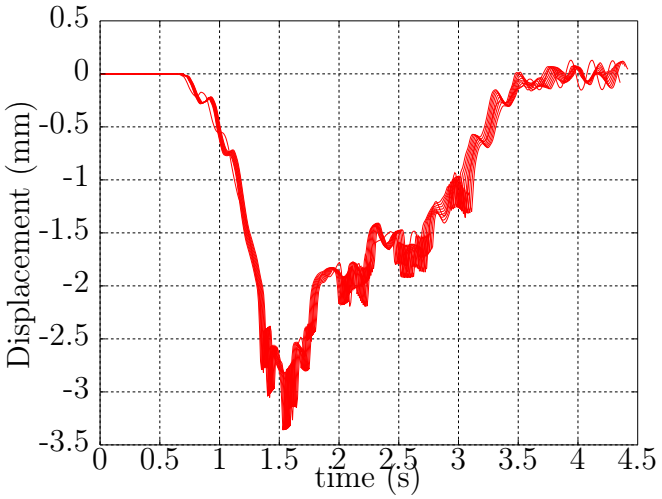

(b) Time variation of displacement for set of velocities between 197 and 206 km/h

Figure 9: Parametric analysis of maximum displacement

Factors (variation)	Key results (vertical) Peak acceleration velocity, displacement
A. Ballast stiffness (40 %)	rail level (a)
B. Ballast mass (6 %)	sleeper level (b)
C. Ballast behaviour (L-NL)	deck level (c)
D. Loads speed (2.7 %)	free rail level (e)
E. Ballast damping (30 %)	soil level (d)
F. Rail pad damping (15 %)	

Table 2: Factors, their variation and key results

The selected factors, their variations and key results are presented in Table 2. The variation of selected factors indicated in Table 2 means that the change is applied to the mean representative value of the model to get the low and high levels. Regarding the ballast mass it is necessary to highlight that the objective is to analyse uncertainty of the cone of dynamically activated ballast, thus the variation is applied to these values, and the total ballast mass is maintained constant. Non-activated ballast mass is associated directly to the deck. Dynamically activated ballast mass variation thus induces very low alterations in natural frequencies, since the total mass of the structure is maintained and only some terms are in different positions of the global mass matrix. This factor should be more correctly named as the dynamically activated ballast mass, but for the sake of simplicity it is kept in the following as "ballast mass".

The key results are extracted from the middle point of the middle span of the viaduct at several levels that are placed on a vertical line that passes the external rail of the track that is subjected to the load passage. They are designated as levels (a), (b), (c) and (d) in Figure 10 and Table 2. In addition, one more point is considered at the rail level that is placed close to the middle of the span, but lies between two sleepers and it is designated as the free rail level (e) (see Figure 10 and Table 2).

Two values of the reference train velocity were considered: v_0=185 km/h and v_0=195 km/h. As the speed varies by 2.7 % around the reference velocity, i.e. approximately 5 km/h to each side, the interval from 180 km/h to 200 km/h is covered. A two-level full factorial analysis was accomplished. Such an analysis of the results assumes that by switching only one factor from its low to its high value and fixing the others, the response is symmetrically positioned around the global mean. It is also assumed that by changing the value of one quantitative factor the response evolution is smooth and without internal extremes. In total $2^6 = 64$ runs were performed, leading to a total computing time of 184.5 hours for each reference velocity. The total computing time could have been halved if a fractional factorial analysis was considered. The efficiency of such method has already been proven in previous work by the authors [13]. The drawback is that then there are not enough results to represent correctly the higher interactions that can be used for calculation of the standard error σ, necessary for the deviation plots.

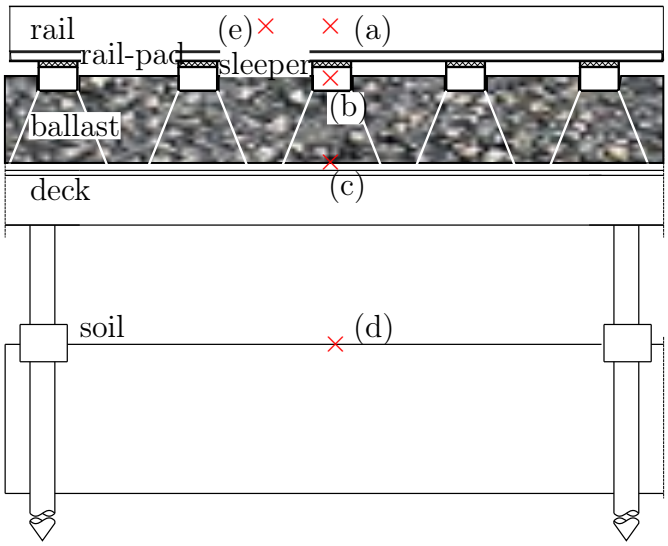

Figure 10: Points of results extraction (not scaled)

The resulting data are output of FE analysis and therefore there is no error associated to experimentation, because the FE results on a model with unchanged parameters are unique.

Only the results exhibiting few dominant single and/or interaction effects are presented, because they are suitable for drawing some conclusions. Consequently, the corresponding response functions are simple and in some cases can be easily visualised. The other results exhibit an excessive amount of significant effects and interactions and therefore are not suitable for drawing valid conclusions and further analyses are required. The selected results are peak acceleration at the free-rail and rail level, peak velocity at the free-rail, peak acceleration at the sleeper, peak velocity at deck and peak displacement at the soil. In addition to the justification above it can be pointed out that velocities at the deck and free rail level were chosen because the former case was the only case where interaction effect exceeded single effects and the latter case was the

only case where ballast behaviour was among the significant effects.

Significant single and combined effects are preferentially visualised with the help of deviation plots (see [18]). They are obtained by plotting the effects calculated on a horizontal axis and setting a reference t-distribution with a number of degrees of freedom (dof) equal to the higher order interactions of the design. Having 63 effects, then 22 of them, the ones that correspond to interactions of 4, 5 and 6 factors, define the number of dof of the distribution and can be used for the standard error σ estimation. The effects that fall outside the reference distribution can be considered as significant, but a better definition of significant effects will be presented later, when the response function will be established. This error is not a measurement error variance but rather an error associated with the interaction of the present factors and with the nature of the result being calculated.

It is confirmed that the standard error is very similar for the same kind of result, when the comparison is made between the lower and higher reference velocity. Regarding the location of the result extraction, the farther the location, the smaller the standard error and thus more significant effects appear. Regarding the type of result, generally, the results presenting less smoothness have a tendency to exhibit a larger variation error, therefore accelerations have higher error than displacements.

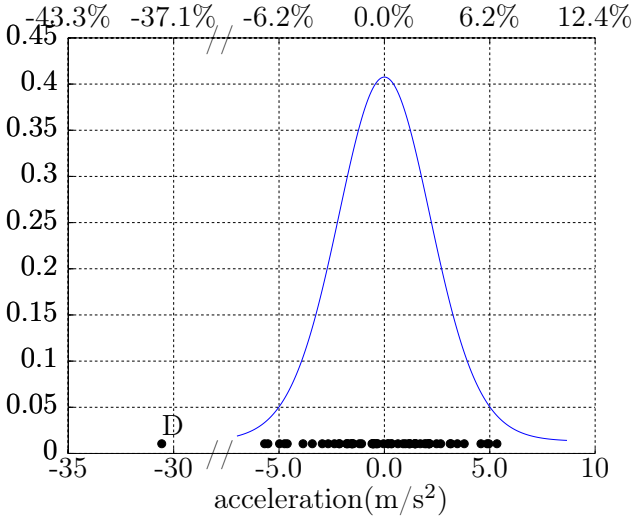

(a) $v_0 = 185$ km/h; $\lambda = 80.83$; $\sigma = 2.23$ m/s^2

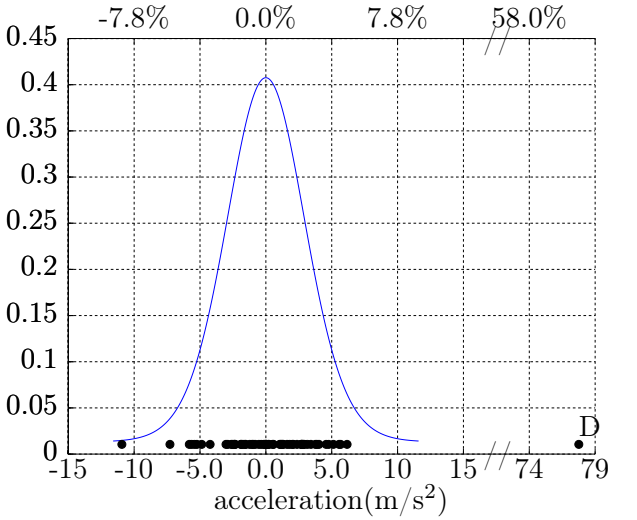

(b) $v_0 = 195$ km/h; $\lambda = 127.64$; $\sigma = 2.99$ m/s^2

Figure 11: Deviation plots of the peak acceleration at the free-rail level

4.2.1. Deviation plots

Deviation plots are shown in Figures 11-14.

It can be concluded from Figure 11 that around the lower reference velocity an increase in velocity within the interval specified decreases the free rail acceleration (by approximately 30 m/s^2); on the other hand around the higher reference velocity an increase in velocity increases significantly (by approximately 75 m/s^2) the free-rail acceleration. At the reference speed of 195 km/h the change in results with increasing velocities can be concluded higher than at the reference speed 185 km/h.

For the rail acceleration there is only one significant effect visible at higher reference velocity (see Figure 12). An increase in value of the rail pad damping within the interval specified decreases the acceleration by almost 10 m/s^2.

In both previous cases the effects that fall outside the distribution are singular effects (with no additional interactions). Those factors (D-load speed and F-rail pad damping) have unequivocally a direct influence on the peak accelerations at the rail and free-rail level. When considering the free-rail peak velocity and sleeper peak acceleration, see Figures 13 and 14, interactions are significant and therefore the singular effects cannot be evaluated separately. Better insight into real dependencies can be given by a two-way ta-

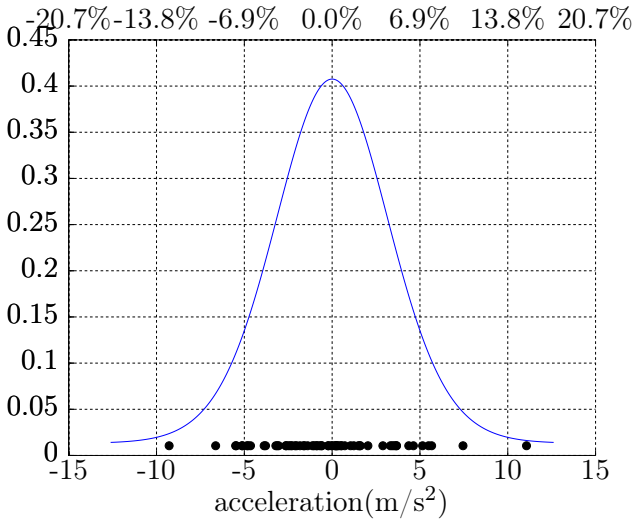

(a) $v_0 = 185$ km/h; $\lambda = 72.56$; $\sigma = 3.25$ m/s^2

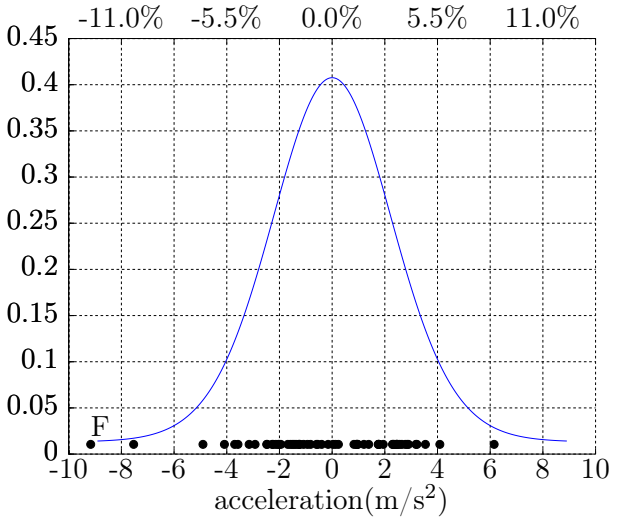

(b) $v_0 = 195$ km/h; $\lambda = 72.42$; $\sigma = 2.30$ m/s^2

Figure 12: Deviation plots of the peak acceleration at the rail level

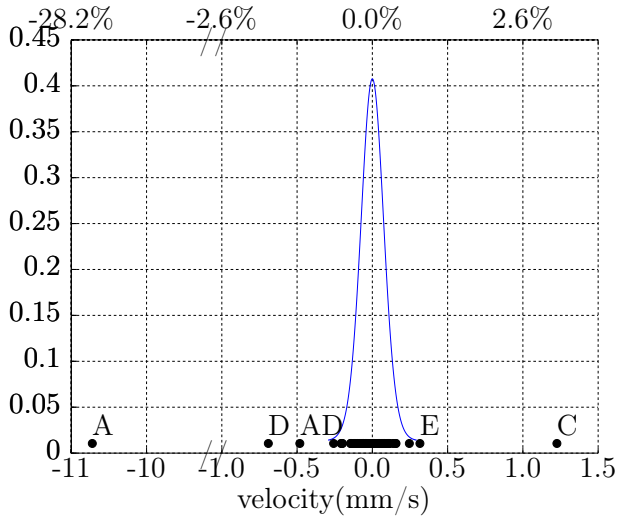

(a) $v_0 = 185$ km/h; $\lambda = 39.1$; $\sigma = 0.076$ mm/s

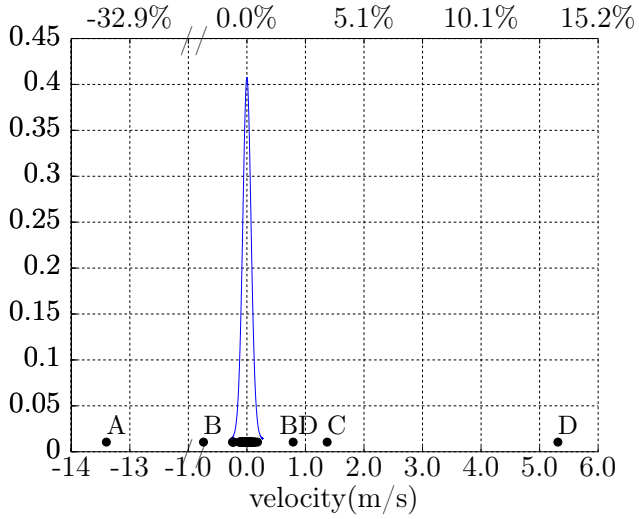

(b) $v_0 = 195$ km/h; $\lambda = 39.5$; $\sigma = 0.071$ mm/s

Figure 13: Deviation plots of the peak velocity at the free rail level

ble of interaction presented in the next section. This is important for the lower reference velocity, where only single effects A and D and their interaction AD are significant.

4.2.2. Half normal plots and interaction tables

When the standard error is very low, the associated normal distribution is very narrow, and the visualisation could be compromised. In these cases the half normal plots were used instead, for the sake of better visualisation. However, the disadvantage of these plots is that the significant effects are presented in an absolute value, therefore direct conclusions if a selected significant effect induces an increase or decrease of the result analysed cannot be taken.

In this section the peak velocity at the sleeper level and the peak displacement at the soil level are presented (Figures 15 and 16).

Regarding the peak velocity at the deck level, it is seen that the dominant effects are the ballast mass, (factor B), the load speed (factor D) and their interaction. Around the lower reference velocity (Figure 15a) the combined effect exceeds the single effects. This graph clearly demonstrates that the interaction effects can be more important than single effects, and therefore key parameters cannot be analysed individually.

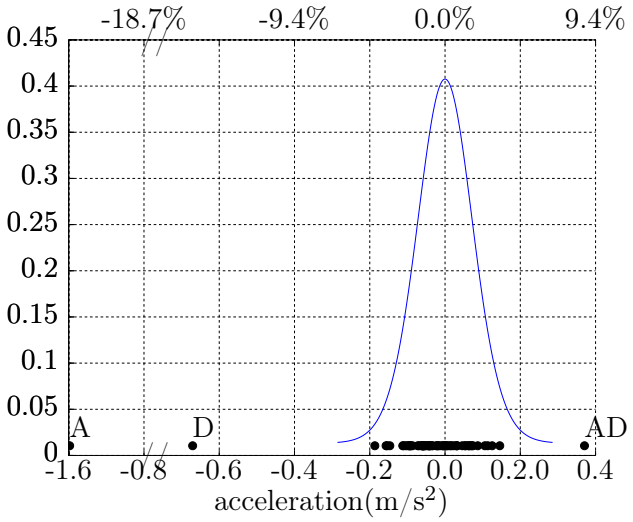

(a) $v_0 = 185$ km/h; $\lambda = 4.27$; $\sigma = 0.07$ m/s^2

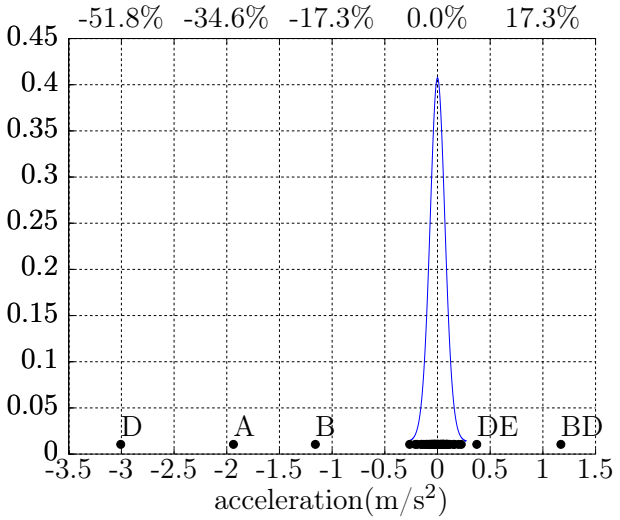

(b) $v_0 = 195$ km/h; $\lambda = 5.79$; $\sigma = 0.07$ m/s^2

Figure 14: Deviation plots of the peak acceleration at the sleeper level

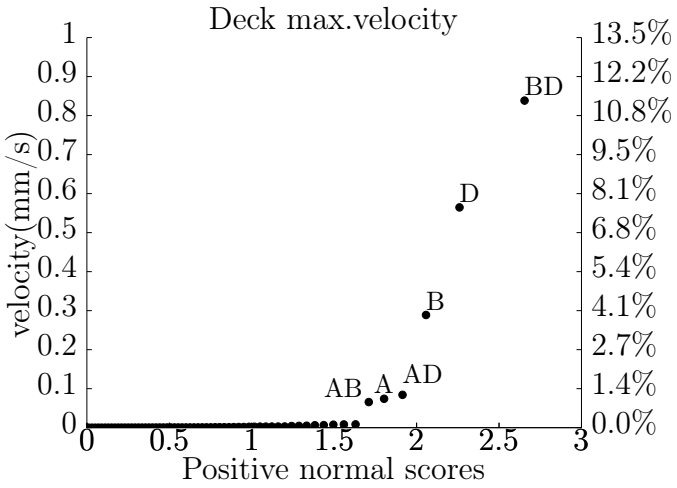

(a) $v_0 = 185$ km/h; $\lambda = 7.4$; $\sigma = 1.0 \times 10^{-3}$[mm/s

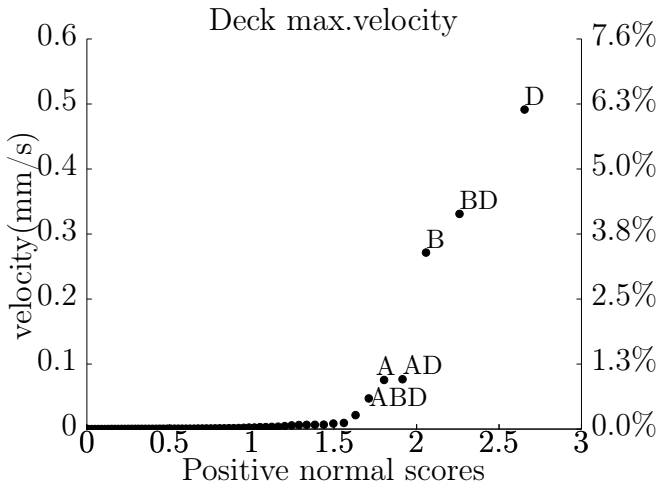

(b) $v_0 = 195$ km/h; $\lambda = 7.9$; $\sigma = 1.5 \times 10^{-3}$ mm/s

Figure 15: Half normal plot of the peak velocity at the deck level

While this is true for the lower reference velocity for the higher reference velocity the load velocity overpasses this interaction. Fourteen combinations are significant in both cases (only the first six are designated in the graph for the sake of clarity).

Both results exhibit a significant interaction. In such cases the two-way interaction tables can provide better insight to these results, see Figure 17a.

It is seen that none of the effects has unequivocal influence in the lower reference velocity, but for the higher reference velocity, Figure 17b, the load speed (factor D) always increases the deck peak velocity.

It can be concluded, that in both results there is an effect of the ballast mass (B), the loads speed (D) and their interaction. It is also seen that the graphs for both reference velocities are very similar, i.e. they are not affected by the reference velocity.

In summary, results revealed that the factors A (the ballast stiffness) and D (the loads speed), and the interaction BD (the interaction of ballast mass and loads speed) are the most important single and combined effects, supporting previous conclusions from [13] and justifying that further research should be conducted in this direction. The objective (ii) from the Introduction is supported by the peak velocity at the deck level at

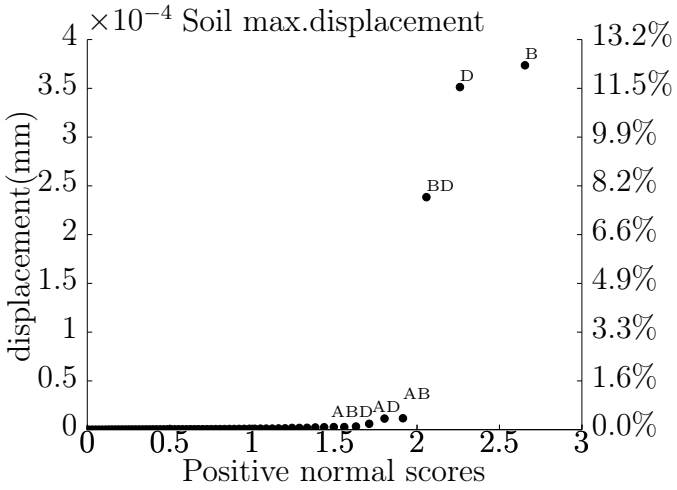

(a) $v_0 = 185$ km/h; $\lambda = 3.0 \times 10^{-3}$; $\sigma = 6.3 \times 10^{-7}$ mm

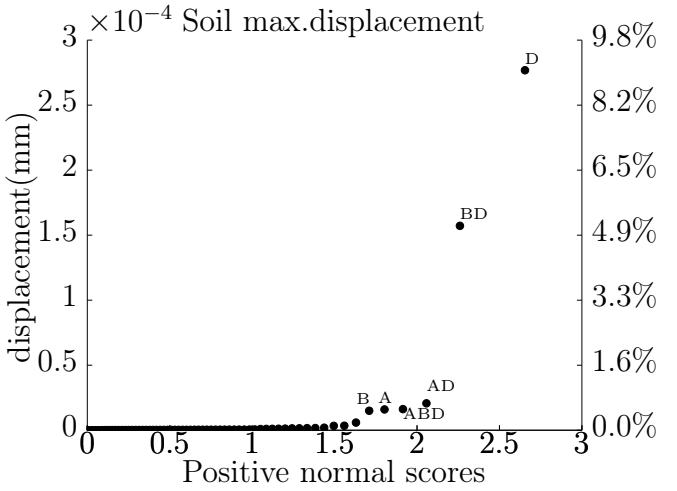

(b) $v_0 = 195$ km/h; $\lambda = 3.1 \times 10^{-3}$; $\sigma = 5.3 \times 10^{-7}$ mm

Figure 16: Half normal plot of the peak displacement at the soil level

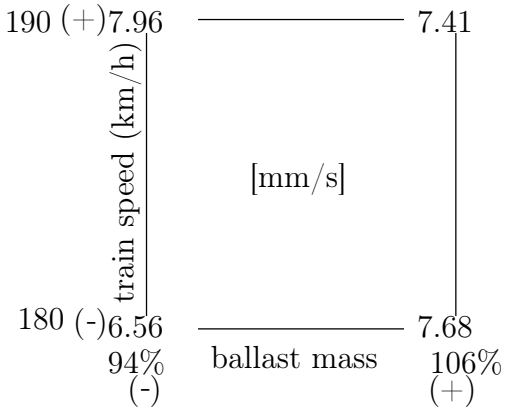

(a) The BD interaction $v_0 = 185$ km/h

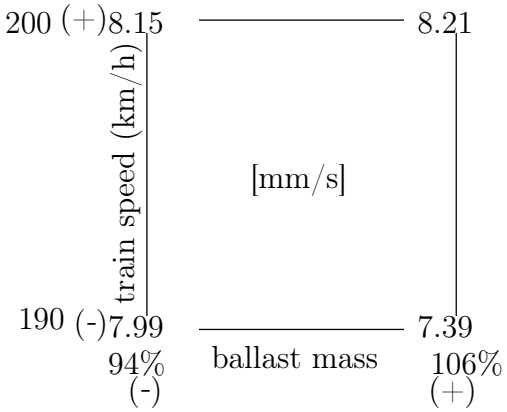

(b) The BD interaction $v_0 = 195$ km/h

Figure 17: Interaction tables, deck peak velocity

the lower reference velocity (Figure 15a); in this case the interaction BD, i.e. the ballast mass with the loads speed is the most relevant effect. All factors selected for the analysis in this paper can be found at some relevant positions in the figures presented, justifying that none one them could be omitted in the factorial screening.

4.2.3. Polynomial response function

For the determination of the response function it is necessary to separate the significant and insignificant effects in a more accurate way.

Significant effects and interactions are defined as the ones that overpass in absolute value the "simultaneous margin of error (SME)", defined as the horizontal coordinate (measured from the zero mean) of the t-student distribution that encompasses the probability of $\phi = (1 + 0.95^{(1/n)})/2$, where n is the number of effects, i.e. $2\phi - 1$ confidence interval. In our case of 63 effects and 22 degrees of freedom $\phi = 99.96$ % and $SME = t_{\phi,dof}\ \sigma = 3.8769\ \sigma$.

The general equation of the response function is

$$y^* = \lambda + \sum_{i=1}^{k} \eta_{x_i} x_i/2 + \sum_{i,j=1\ \ i>j}^{k} \eta_{x_i x_j} x_i x_j/2 + \cdots \quad (6)$$

where η are the effects, k is the number of factors and x represent the scaled factors with the value variation from low to high level $-1 \leq x \leq 1$.

Only the significant effects should be used in the equation above. The response function can be used for calculation of the expected response. The most easily interpretable response functions are the ones where only two effects and their interaction are significant, because then they can be graphically visualised.

From Equation (6) it is seen, that when there are no significant interactions, then the response is linear, i.e. the response at the mean value of a factor should approximately equal the average of the responses at the low and high level of this particular factor. When interactions are present, then quadratic, cubic and even higher order terms appear. Nevertheless, the response function can be considered valid, if the assumption for the full factorial analysis stated in Section 4.2 is verified.

The response functions of the results are shown next; a, v and u stand for the acceleration, velocity and the displacement, acceleration is presented in m/s^2, but velocity and displacement in mm/s and mm, respectively. Superscript (a), (b), (c), (d) and (e) represent the points of the results extraction (see Figure 10) and subscript 185 or 195 stand for the reference velocity. The functions are presented in the same order as in the previous subsections.

The peak acceleration of the free-rail is given by:

$$\begin{aligned} a^{(e)}_{185}* =& 80.83 - 15.28x_D \qquad (7)\\ a^{(e)}_{195}* =& 127.60 + 37.88x_D \end{aligned}$$

which are linear functions of the variable x_D representing the load velocity factor. Similarly the rail peak acceleration is given by

$$a^{(a)}_{195}* = 72.42 - 4.58x_F \qquad (8)$$

that is valid for the higher reference velocity. For the lower reference velocity the function cannot be presented because there are no significant effects.

The free-rail peak velocity, involving all five significant effects is given by the functions

$$\begin{aligned} v^{(e)}_{185}* =& 39.00 - 5.00x_A + 0.61x_C - 0.35x_D \qquad (9)\\ & -0.24x_Ax_D + 0.16x_E \\ v^{(e)}_{195}* =& 39.00 - 5.10x_A + 2.70x_D + 0.69x_C \qquad (10)\\ & +0.39x_Bx_D - 0.37x_B \end{aligned}$$

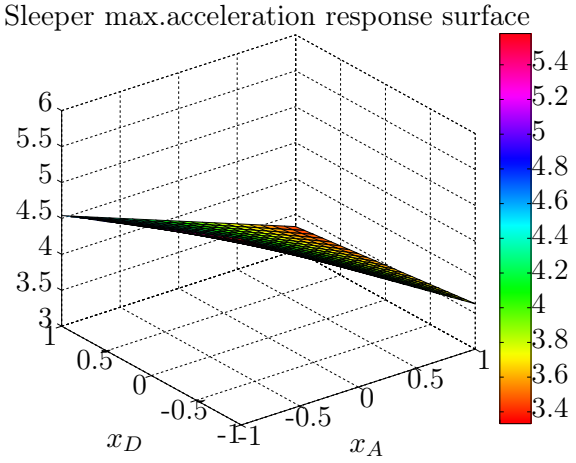

Figure 18: $v_0 = 185$ km/h

Further, the sleeper peak acceleration has three and five significant effects and interactions for the reference velocity of 185 km/h and 195 km/h, respectively, as can be verified in Figure 14. The respective response functions are given by:

$$\begin{aligned} a^{(b)}_{185}* =& 4.27 - 0.79x_A - 0.34x_D \qquad (11)\\ & +0.19x_Ax_D \\ a^{(b)}_{195}* =& 5.80 - 1.50x_D - 0.97x_A + \qquad (12)\\ & +0.59x_Bx_D - 0.58x_B + 0.18x_Dx_E \end{aligned}$$

For the first reference velocity this function can be fully represented graphically since only two effects and their combination appear as significant, see Figure 18.

For the deck velocity response function only the first six and seven effects (from the total of 14) are presented for the lower and higher reference velocity. The remaining significant effects have relative contribution less than 0.1 % and are

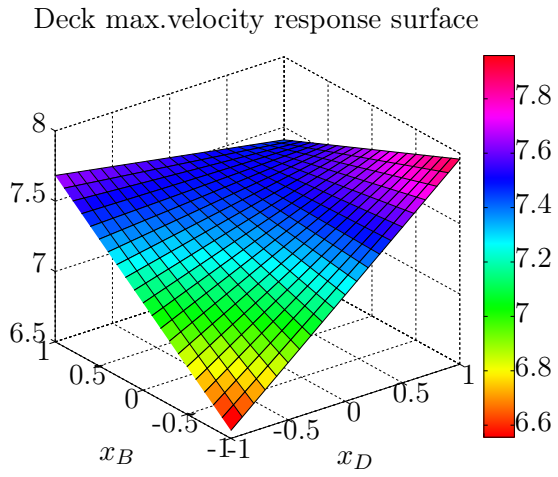

(a) $v_0 = 185$ km/h

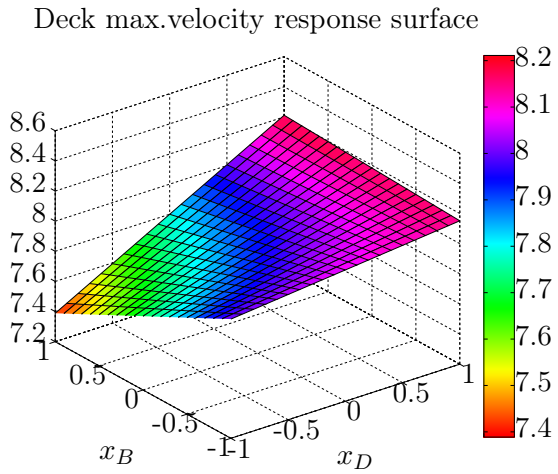

(b) $v_0 = 195$ km/h

Figure 19: Response surface from peak velocity at the deck level

therefore omitted.

$$v_{185}^{(c)}* = 7.40 - 0.42x_Bx_D + 0.28x_D + 0.14x_B + 0.04x_Ax_D + 0.04x_A - 0.03x_Ax_B \quad (13)$$

$$v_{195}^{(c)}* = 7.90 + 0.25x_D + 0.17x_Bx_D - 0.14x_B - 0.04x_Ax_D + 0.04x_A + 0.02x_Ax_Bx_D - 0.01x_Ax_B \quad (14)$$

For the same reason only five and six effects (from the total of 14) are shown in the response functions of the soil displacement for higher and lower reference speed, respectively:

$$u_{185}^{(d)}* = (3.00 + 0.190x_B + 0.180x_D - 0.120x_Bx_D + 0.006x_Ax_B - 0.006x_Ax_D) \times 10^{-3} \quad (15)$$

$$u_{195}^{(d)}* = (3.10 - 0.140x_D - 0.079x_Bx_D + 0.010x_Ax_D - 0.008x_Ax_Bx_D + 0.008x_A - 0.008x_B) \times 10^{-3} \quad (16)$$

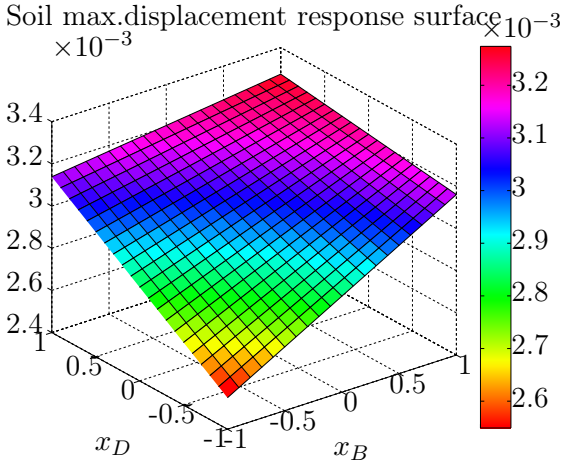

(a) $v_0 = 185$ km/h

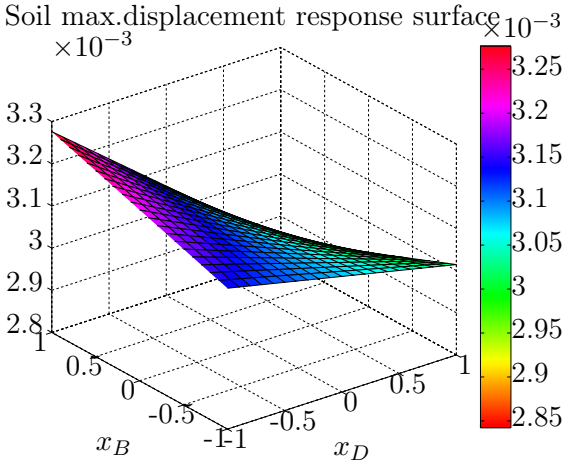

(b) $v_0 = 195$ km/h

Figure 20: Response surface of peak displacement at the soil level

Graphical representation of Equations (13)-(16) is not possible. However, if the influence of ballast stiffness (A) and its interactions are removed, then the functions with the remaining terms can

be visualised and are shown in Figures 19 and 20. This graphical approach is naturally more accurate when only significant effects are considered. Then Figure 18 is more accurate than Figures 19 and 20 because there are no significant effects neglected. On the other hand, for instance, velocity at the deck level for the lower reference velocity has 14 significant effects and interactions. This is not very clear from Figure 15a, but they are: BD, D, B, AD, A, AB, ABD, BC, CD, C, BE, ABE, ABC and AC. In Figure 19a only the first three significant effects are included. Nevertheless, looking at Equation (13), one can see that the effects represented are much higher than the ones neglected and therefore Figures 19 and 20 also stand for a useful representation of the expected results.

4.2.4. Residuals plots

The response function is estimated from the significant single effects and interactions. Then the difference between the estimated and calculated values (or residuals) should be validated. Residual plots are shown in Figures 21-26. All points representing the residuals should obey normal distribution and thus closely fit the dashed (error) line in Figures 21-26 and not exhibit high concentrations in specific locations away from the mean. This check is an important step in the validation of the response function. The residuals are calculated using all significant effects, even if some of them are not included in the equations for the response function for the sake of simplicity, or in the response surface plots, where including more effects is impossible.

In some cases it is seen that there are some values that the response function cannot recover perfectly well (Figures 22 and 24b), but, with consideration of the next significant effect, residuals would fit closely to the reference line.

The residual check is valuable provided that the number of significant effects is small compared with the total number of combinations. In our case the highest number of significant effects is 14 (results of the peak velocity at the deck level and the peak displacement at the soil level) and the total number of combinations is 64, giving

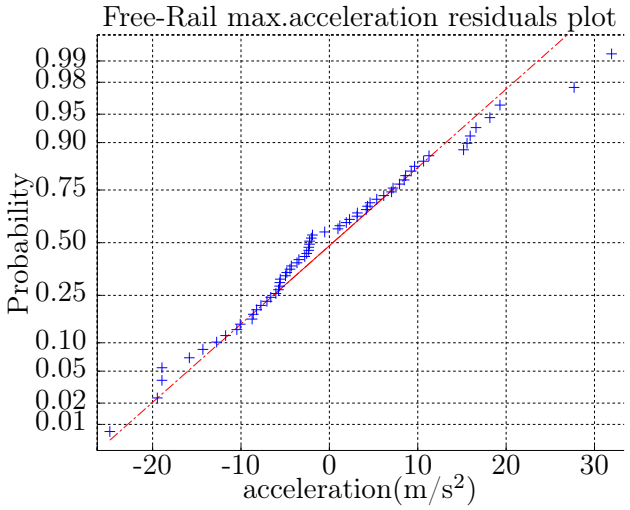

(a) $v_0 = 185$ km/h

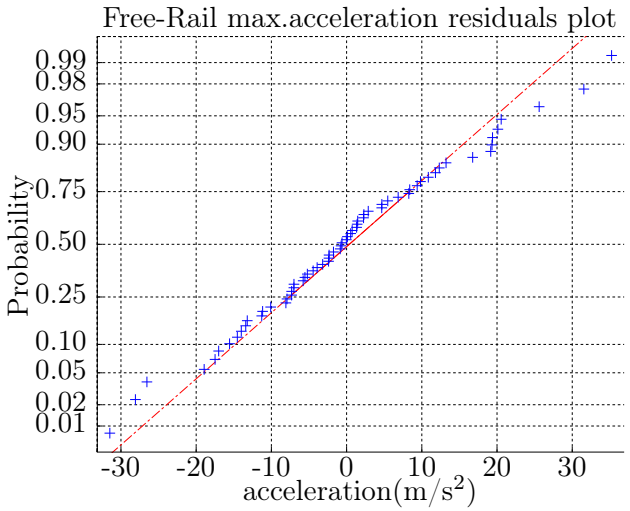

(b) $v_0 = 195$ km/h

Figure 21: Residuals plots of the peak acceleration at the free rail level

an acceptable ratio of 22 %. In summary, it was demonstrated that the residuals are well-behaved and therefore the conclusions taken in this paper are meaningful.

For the sake of comparison, residuals related to the graphical representation in Figures 19 and 20, i.e. calculated as if only three or two significant effects were included in the response function, are plotted over the original residuals in Figures 25 and 26. It is seen that with reduced number of factors the slope is much lower, i.e. the standard deviation of residuals, is much higher. But the residuals are still quite close to the error line with no noticeable concentrations away from the mean

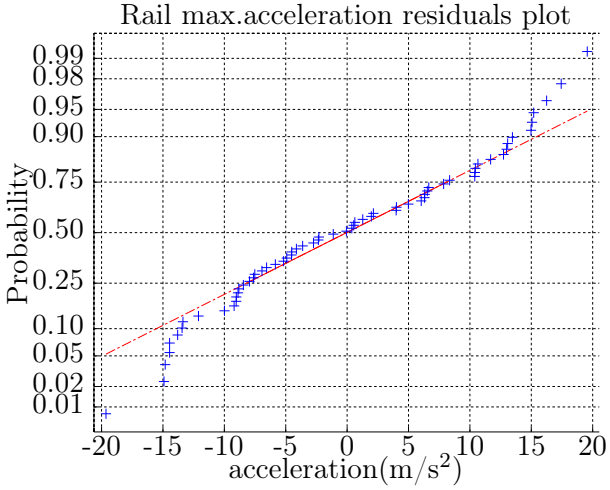

Figure 22: $v_0 = 195$ km/h

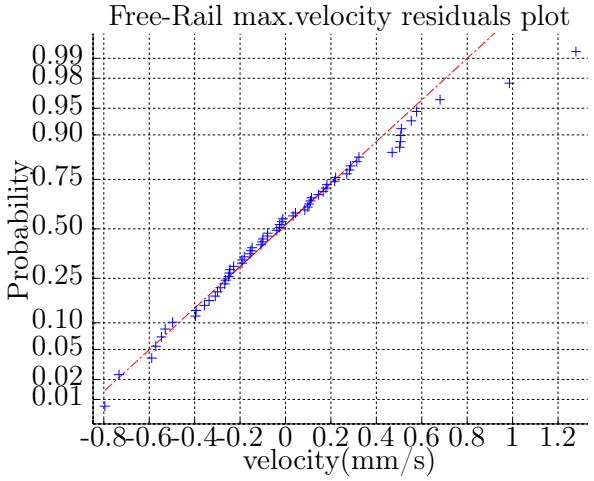

(a) $v_0 = 185$ km/h

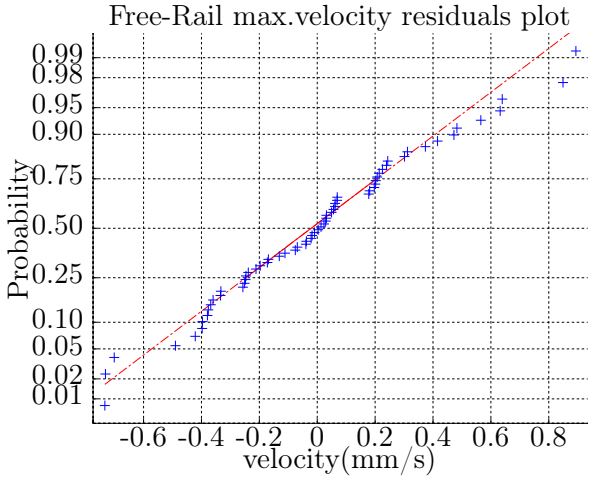

(b) $v_0 = 195$ km/h

Figure 23: Residuals plots of the peak velocity at the free rail level

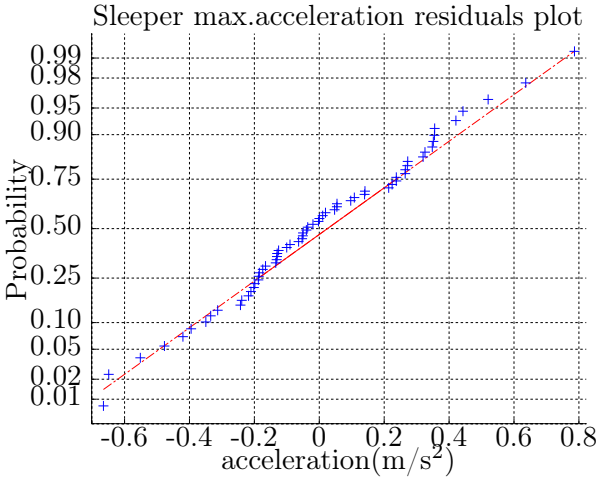

(a) $v_0 = 185$ km/h

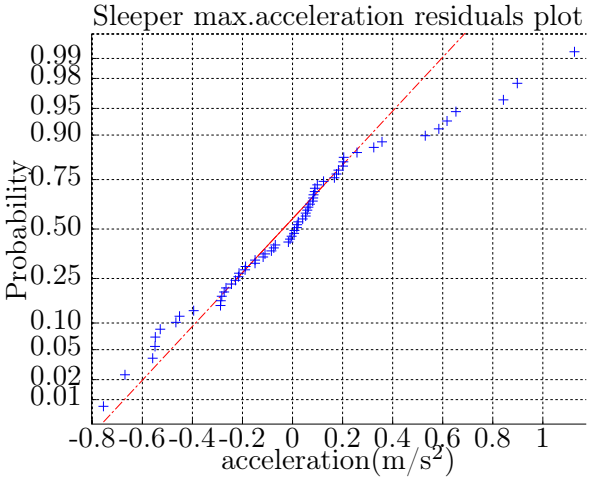

(b) $v_0 = 195$ km/h

Figure 24: Residuals plots of the peak acceleration at the sleeper level

region, justifying the usage of simplified response functions as well.

The conclusions taken are valid only on the intervals considered. In the present case, the intervals represent the uncertainties, and therefore are fixed. The load velocity is the factor that is more flexible and thus it was useful to see how the conclusions are altered for higher and lower velocities, which was the topic discussed in detail in previous sections.

4.2.5. Probability of exceedance of a certain result

The statistical analysis shown in previous sections makes no assumption on the distribution of a certain input value (factor) within the interval specified. Randomly selected input data within

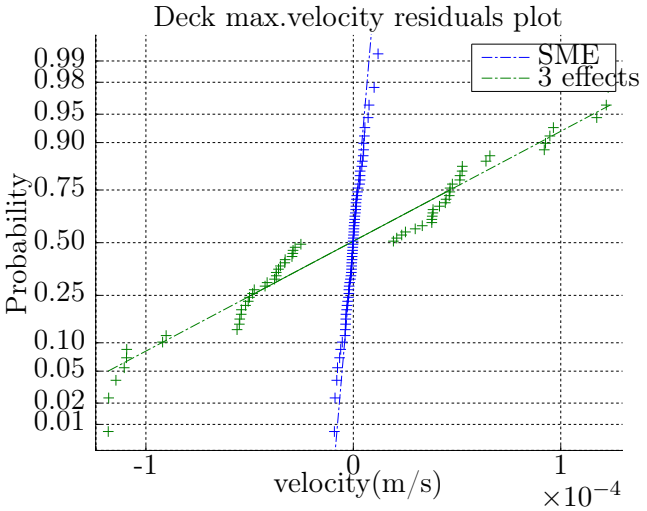

(a) $v_0 = 185$ km/h

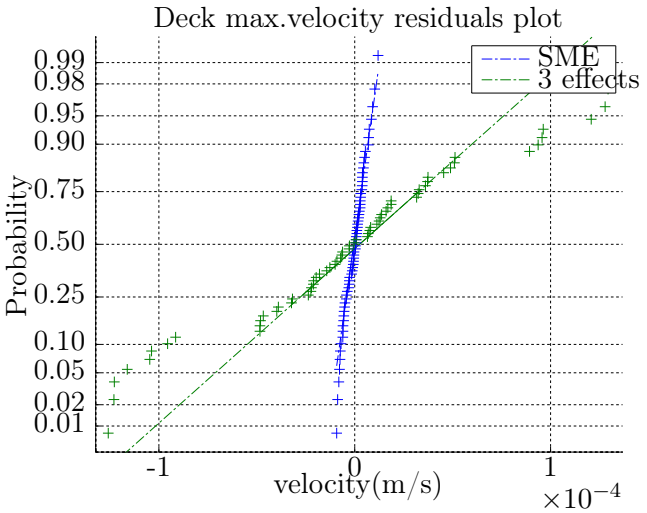

(b) $v_0 = 195$ km/h

Figure 25: Residuals plots of the peak velocity at the deck level

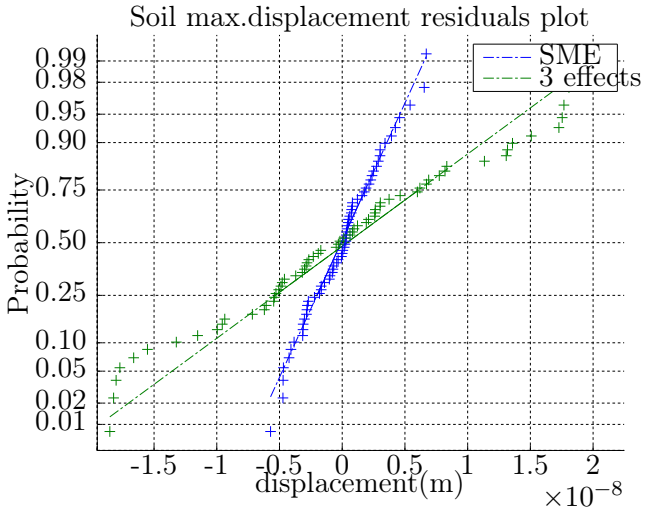

(a) $v_0 = 185$ km/h

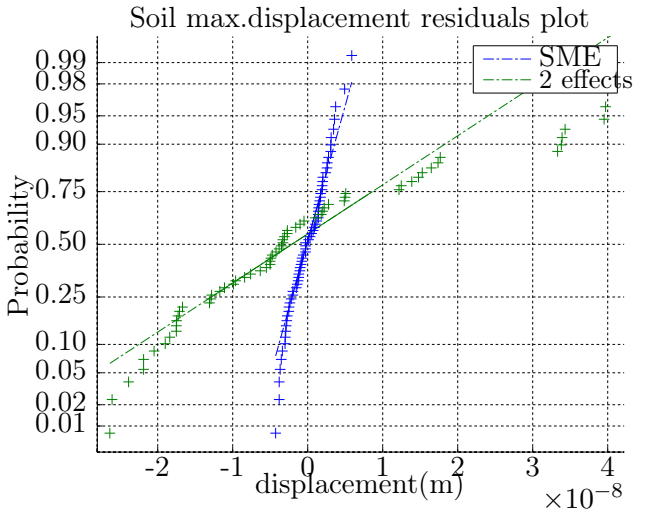

(b) $v_0 = 195$ km/h

Figure 26: Residuals plots of the peak displacement at the soil level

these intervals would exhibit uniform probability over the interval. It is assumed that the variation of the factors represents the input data uncertainties, and therefore the real value obeys the normal distribution, encompassing the interval considered. Then the response functions can be used for calculation of a probability of exceedance of a certain value. The method of calculation of this probability can be explained in a simple case. Consider that only two factors, x_1 and x_2 are involved and the value of interest is y_0. Moreover assume that by solving

$$y^*(x_1, x_2) \geq y_0 \tag{17}$$

an explicit function can be obtained and the condition above is verified for

$$x_2 \geq f(x_1) \tag{18}$$

Let also the function $f(x_1)$ intersect the axis x_1 within the interval [-1,1] in at most two values, $x_{1d} < x_{1u}$. Then the probability that the value y_0 will be exceeded can be calculated by

$$p = \int_{\max(-1,x_{1d})}^{\min(1,x_{1u})} F(x_1) \left(\int_{\max(-1,f(x_1))}^{1} F(x_2) \mathrm{d}x_2 \right) \mathrm{d}x_1 \tag{19}$$

where $F(x_i)$ is the normal distribution function

that is attributed to the uncertainty and $i = 1, 2$. Values -1 and 1 are preferentially used in Equation (19) because the response function may not be valid outside these limits. The standard deviation is defined in the way that the accuracy is acceptable.

As an example, the probability that the deck peak velocity exceeds 7.4 mm/s and 8 mm/s for the lower and the higher reference velocity, respectively, is calculated. The deck peak velocity is given by Equations (13) and (14). With all effects neglected, except for B (ballast mass), D (load velocity), and BD this dependence was shown in Figures 17 and 19. In order to implement Equation (19), it is necessary to assume that the train velocity complies with the reference value and the deviations obey the normal distribution. It is assumed that the representative distribution within the interval -1 and 1 has the standard deviation of 1/3, i.e. the encompassing probability within the interval is 99.73 %. Using Equations (13) and (14) it is possible to solve the inequality from Equation (18) and calculate the probability as 56.5 % and 14.2 %, respectively.

Equation (19) can be extended to more factors.

5. Conclusions

A complete statistical analysis, based on a two-level factorial design of experiments was presented and several analysis tools were applied to a real case study. The statistical theory proved to be relevant, meaningful and easy to implement.

The main conclusions are listed as: (i) Although the ballast constitutive law appeared as a significant effect only in one result, this is sufficient to conclude that this factor should not be overlooked. (ii) Interaction effects can be more important than single effects, and therefore key parameters cannot be analysed individually. This is supported by the peak velocity at the deck level at the lower reference velocity (Figure 15a); in this case the interaction BD, i.e. the ballast mass with the load speed is the most relevant effect. (iii) Response functions can be easily constructed and used for results representation and estimation, as well as for determination of the probability that a certain result of interest will exceed a specified value. In the latter case is must be assumed that the factors variation corresponds to a range of uncertainties and obeys the normal distribution within the interval specified.

In this paper the importance was given to the superstructure modelling parameters. It was shown that several significant effects and interactions exists, and therefore, as a conclusion, it must be stressed that the railway viaduct superstructure has to be modelled with sufficient accuracy. All factors selected can be found at some relevant positions in the figures of the previous sections, justifying that none one them could be omitted in the factorial screening. Thus none of the superstructure construction details should be neglected or highly simplified. Attention must be paid to the estimate of dynamically activated ballast mass and correct, non-linear, ballast behaviour.

In summary, it has been shown how useful the statistical analysis can be, and how it can be implemented on existing structures. It is known that the method is not able to explore fully a wide region in the factor space, but it can indicate trends and directions for further exploration. For example, the implementation of this analysis with a response surface algorithm, capable of analysing a given model and output the dynamic response surface would add accuracy on the bridge design analysis and to prospective in-situ measurements.

6. Acknowledgements

The authors greatly appreciate support from Fundação para a Ciência e a Tecnologia of the Portuguese Ministry of Science and Technology, supporting this work through the project grant PTDC/EME-PME/01419/2008: "SMARTRACK - SysteM dynamics Assessment of Railway TRACKs: a vehicle-infrastructure integrated approach" and "PTDC/ECM/115932/2009: Adaptive methods for reliability analysis of complex structures".

References

[1] Yang YB, Yau JD, Wu YS. Vehicle-Bridge Interaction Dynamics: With Applications To High-Speed Railways. World Scientific; 2004. ISBN 9789812388476.

[2] Frýba L. Dynamics of railway bridges. London: T. Telford; 1996. ISBN 9780727720443.

[3] Inglis C. A Mathematical Treatise on Vibrations in Railway Bridges. The Cambridge University Press; 1934.

[4] Frýba L. Vibration Of Solids And Structures Under Moving Loads. London: Thomas Telford; 3^{rd} ed.; 1999. ISBN 9780727727411.

[5] Biondi B, Muscolino G, Sofi A. A substructure approach for the dynamic analysis of train-track-bridge system. Computers & Structures 2005;83(28-30):2271–81. doi:10.1016/j.compstruc.2005.03.036.

[6] Pesterev A, Yang B, Bergman L, Tan C. Revisiting the moving force problem. Journal of Sound and Vibration 2003;261(1):75 – 91. doi:10.1016/S0022-460X(02)00942-2.

[7] Chan TH, Ashebo DB. Theoretical study of moving force identification on continuous bridges. Journal of Sound and Vibration 2006;295(3–5):870 – 883. doi:10.1016/j.jsv.2006.01.059.

[8] Bilello C, Bergman L, Kuchma D. Experimental investigation of a small-scale bridge model under a moving mass. Journal of Structural Engineering 2004;130(5):799–804. doi:10.1061/(ASCE)0733-9445(2004)130:5(799).

[9] Akin J, Mofid M. Numerical solution for response of beams with moving mass. Journal of Structural Engineering 1989;115(1):120–131. doi:10.1061/(ASCE)0733-9445(1989)115:1(120).

[10] Xia H, Xu Y, Chan TH, Zakeri J. Dynamic responses of railway suspension bridges under moving trains. Scientia Iranica 2007;14(5):385–394.

[11] Lee C, Kawatani M, Kim C, Nishimura N, Kobayashi Y. Dynamic response of a monorail steel bridge under a moving train. Journal of Sound and Vibration 2006;294(3):562 – 579. doi:10.1016/j.jsv.2005.12.028.

[12] Tan C, Shore S. Response of horizontally curved bridge to moving load. In: Journal of the Structural Division ASCE; vol. 94. 1968, p. 2135–2154.

[13] Jesus AH, Dimitrovová Z, Silva MAG. Qualitative influence of model parameters on the dynamic response of a viaduct. International Journal of Railways Technology 2012;1(2):89–113. doi:10.4203/ijrt.1.2.5.

[14] Wiberg J, Karoumi R, Pacoste C. Statistical screening of individual and joint effect of several modelling factors on the dynamic finite element response of a railway bridge. Computers and Structures 2012;106(0):–. doi:10.1016/j.compstruc.2012.04.008.

[15] Karalar M, Padgett JE, Dicleli M. Parametric analysis of optimum isolator properties for bridges susceptible to near-fault ground motions. ENGINEERING STRUCTURES 2012;40:276–287.

[16] Fang SE, Perera R. A response surface methodology based damage identification technique. Smart Materials and Structures 2009;18(6):065009.

[17] Fang SE, Perera Velamazán R. Damage assessment of a full-scale bridge based on the response surface method. In: Proceedings of the Eleventh International Symposium on Structural Engineering. Guangzhou, China; 2010,.

[18] Box G, Hunter W, Hunter J. Statistics for experimenters: an introduction to design, data analysis, and model building. Wiley series in probability and mathematical statistics: Applied probability and statistics; Wiley; 1978. ISBN 9780471093152.

[19] Czitrom V. One-factor-at-a-time versus designed experiments. The American Statistician 1999;53(2):126–131.

[20] Schabenberger O, Gregoire TG, Kong F. Collections of simple effects and their relationship to main effects and interactions in factorials. The American Statistician 2000;54(3):210–214. doi:10.1080/00031305.2000.10474547.

[21] Siringoringo DM, Fujin Y. Estimating Bridge Fundamental Frequency from Vibration Response of Instrumented Passing Vehicle: Analytical and Experimental Study. ADVANCES IN STRUCTURAL ENGINEERING 2012;15(3):417–433.

[22] REFER . Projecto de modernização da linha do norte sub-troço 1.4: Azambuja(excl.) - vale de santarém(incl.), projecto de execução, volume 10 - viaduto santana do cartaxo, memória descritiva e justificativa – geologia e geotecnia, memória descritiva e justificativa – obra de arte revisão 1, viaponte(in portuguese). Tech. Rep.; Estradas Portugal EP; September 2003.

[23] Swanson Analysis Systems IP I. ANSYS, Inc. Documentation for Release 12.1; 2009.

[24] Mazilu T, Dumitriu M. On the Steady State Interaction between an Asymmetric Wheelset and Track. In: Topping BHV, Tsompanakis Y, editors. Thirteenth International Conference on Civil, Structural and Environmental Engineering Computing. Stirlingshire, Scotland; 2011,doi:10.4203/ccp.96.27.

[25] Dahlberg T. Dynamic interaction between train and non-linear railway track model. In: Structural Dynamics: EURODYN 2002 : Proceedings of the 4th [i.e. 5th] International Conference on Structural Dynamics, Munich, Germany, 2-5 September 2002. v. 2; Balkema; 2002,.

[26] Dimitrovová Z, Rodrigues A. Critical velocity of a uniformly moving load. Advances in Engineering Software 2012;50:44–56.

[27] The MathWorks . Matlab online documentation. [online]; 2009. URL http://www.mathworks.com/access/helpdesk/help/techdoc/.

[28] Zhai W, Wang K, Lin J. Modelling and experiment of railway ballast vibrations. Journal of Sound and Vi-

bration 2004;270(4–5):673 – 683. doi:10.1016/S0022-460X(03)00186-X.
[29] Lysmer J, Kuhlemeyer R. Finite dynamic model for infinite media. In: Journal of the Engineering Mechanics Division, ASCE. 95(EM4); 1969, p. 859–877.

Appendix A. Geological data

The following Table A.3 summarises all the relevant geological information of the viaduct surrounding soil.

Geo-technical unit	μ [kN/m^3]	G[MPa] $\gamma = 10^{-6}$	10^{-4}	10^{-3}	ν	E[MPa] 10^{-4}	10^{-3}
"A1"	16	19.8	19.8	10.9	0.49	59	32.5
"A2" and "A3"	18	36	28.8	14.4	0.35	77.7	38:9
Pleistocene and Miocene	20	66.1	59.5	36.4	0.48	176.1	107.7
Miocene	21.5	350	298	157	0.25	745	392.5

Table A.3: Geological data (estimated)

μ, G, ν, γ and E stand for the specific weight, distortion modulus, Poisson's coefficient, distortion and Young's modulus, respectively. Dependency on distortion was neglected and an average value was used instead.

Appendix B. Geometrical data

In this section geometrical data of the railway and viaduct deck are presented.

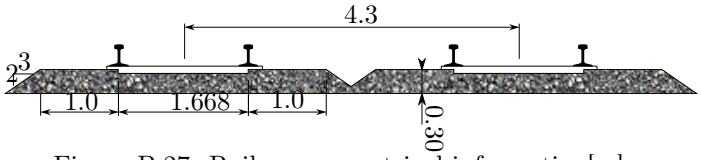

Figure B.27: Railway geometrical information[m]

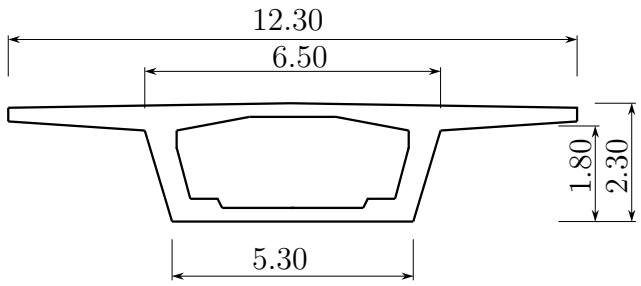

Figure B.28: Viaduct deck section geometry [m]

Appendix C. Material data

The relevant material data are presented in the following Tables C.4 - C.6. They refer to the rail properties (Table C.4), concrete parts properties (Table C.5) and spring and damper parameters of the superstructure arrangement (Table C.6).

Property	(UIC60)
Young's modulus E (GPa)	210
Poisson's ratio ν	0.3
Density ρ (kg/m^3)	7800
Cross-section area A (m^2)	$76.84 \cdot 10^{-4}$
Moment of inertia I (m^4)	$3055 \cdot 10^{-8}$

Table C.4: UIC60 rail data

Material	E (GPa)	ν	ρ (ton/m^3)	model part
C3037	33	0.3	2.5	pillars
C4555	36	0.3	2.5	piles, deck, foundation
PSC	30	0.2	2.054	sleepers

Table C.5: Material data for concrete parts

C3037 and C4555 designate the concrete class and PSC stands for the prestressed concrete.

Spring and damper parameters of the superstructure arrangement referred in Figure 4 are summarised in the Table C.6 bellow. The ballast mass was calculated using the given density of 1.8 ton/m^3. The concentrated mass in Table C.6 corresponds to the cone represented in Figure 10, i.e. to the part of ballast that is dynamically activated by the moving load under each sleeper, estimated according to [28]. The remaining mass of the ballast is distributed uniformly as an additional mass of the viaduct deck.

Springs and dampers that represent the soil removed from the model were estimated as described in [13]. The variation in depth of the spring constants followed the results of the consolidation analysis, represented in Figure C.29. Their values range from 2014.33 to 6453.84 kN/m. These values were also used on the bottom face; in place of part of the piles a stronger spring

Parameter	Value
m_b	0.3225 ton
k_y - ballast	120000 kN/m
c_y - ballast	70 kNs/m
k_x - ballast	40000 kN/m
c_x - ballast	52 kNs/m
k_z - ballast	40000 kN/m
c_z - ballast	52 kNs/m
k_α - ballast	676 kNm
c_α - ballast	394 kNs
k_β - ballast	676 kNm
c_β - ballast	394 kNs
k_y – rail pad	280000 kN/m
c_y – rail pad	50 kNs/m
k_x – rail pad	50000 kN/m
c_x – rail pad	10 kNs/m
k_z – rail pad	50000 kN/m
c_z – rail pad	10 kNs/m
k_α - rail pad	597 kNm
c_α - rail pad	0.107 kNs
k_β - rail pad	597 kNm
c_β - rail pad	0.107 kNs

Table C.6: Ballast and Rail pad parameters

was used. Damping coefficients of the viscous dampers were calculated according to [29]

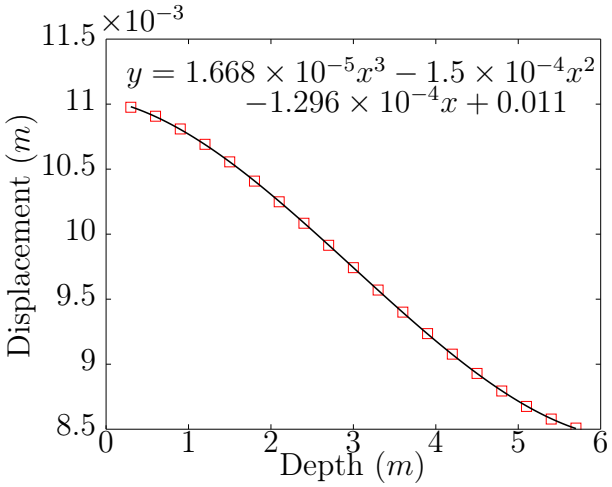

Figure C.29: Cubic trend-line approximation of the displacement originated by uniform unit pressure with respect to depth